ADVANCED OPTICAL MATERIALS

Supporting Information

for *Adv. Optical Mater.*, DOI 10.1002/adom.202302797

High-Index and Low-Loss Topological Insulators for Mid-Infrared Nanophotonics: Bismuth and Antimony Chalcogenides

*Sergey G. Menabde, Jacob T. Heiden, Vladimir A. Zenin, N. Asger Mortensen and Min Seok Jang**

Supporting Information

High-index and low-loss topological insulators for mid-infrared nanophotonics: Bismuth and antimony chalcogenides

Sergey G. Menabde[1], Jacob T. Heiden[1], Vladimir A. Zenin[2], N. Asger Mortensen[3,4], and Min Seok Jang[1,*]

[1]School of Electrical Engineering, Korea Advanced Institute of Science and Technology, 34141 Daejeon, Korea
[2]Center for Nano Optics, University of Southern Denmark, DK-5230 Odense, Denmark
[3]POLIMA – Center for Polariton-driven Light-Matter Interactions, University of Southern Denmark, DK-5230 Odense, Denmark
[4]Danish Institute for Advanced Study, University of Southern Denmark, DK-5230 Odense, Denmark
*Corresponding author: jang.minseok@kaist.ac.kr

S1 Dielectric function of BTS and BSTS crystals

As has been demonstrated in literature, dielectric function of the 2D topological surface layer in BTS[1] and BSTS[2-4] can be modelled by a 2D permittivity in Drude form:

$$\varepsilon_{xy}(\omega) = \varepsilon_1 + i\varepsilon_2 = \varepsilon_\infty - \frac{\omega_p^2}{\omega^2+i\Gamma\omega}, \varepsilon_z = 1,$$

where ε_∞ is the high-frequency dielectric constant, ω_p is the plasma frequency, and Γ is the damping rate. The imaginary part of the dielectric function of a bulk can be approximated by the Tauc-Lorentz model for multiple oscillators[1, 3-4] ($N = 1$ for BSTS and $N = 2$ for BTS):

$$\varepsilon_2^{\mathrm{bulk}}(E) = \sum_{i=1}^{N} \frac{A_i E_{0i} C_i \left(E - E_g\right)^2}{(E^2 - E_{0i}^2)^2 + C_i^2 E^2} \frac{\Theta\left(E - E_g\right)}{E}$$

where Θ is the Heaviside function, E_0 is the peak transition energy of the oscillator, E_g is the bandgap, A is the amplitude of the oscillator, and C is the broadening term. Then, the real part can be obtained from the Kramers-Kronig relations:

$$\varepsilon_1^{\mathrm{bulk}}(E) = \varepsilon_\infty + \frac{2}{\pi} P \int_{E_g}^{\infty} \frac{\xi \varepsilon_2(\xi)}{\xi^2 - E^2} d\xi.$$

Model parameters used in our calculations are adopted from previous works[1-4] and summarized in Table S1.

S2 Dielectric function of BS

Due to the complex nature of states in the bulk BS stemming from the mix of free carriers and multiple phonon modes, the experimentally verified model (like the Tauc-Lorentz model for BTS and BSTS) is still missing. In recent near-field study of BS in THz,[5] its authors mentioned that assuming the in-plane bulk ε = 22 provides a good approximation for dispersion of polaritons in BS. Therefore, we adopted this number which provides agreement with the experimentally measured HPP dispersion (Fig. 2A in main text).

The surface layer of thickness d can be modelled by 2D DC conductivity by Dirac carriers:

$$\sigma_{2D}^{DC} = \frac{e^2 E_F \tau}{d\pi\hbar^2}$$

where $E_F = 0.189$ eV is the Fermi energy, $d = 0.92$ nm is the thickness of the surface layer, and τ = 100 fs is the experimentally measured carrier lifetime[6-7]. Then the in-plane isotropic dielectric function in Drude form[2, 8] is given by:

$$\varepsilon_{xy}(\omega) = \varepsilon_\infty + \frac{i\sigma_{2D}^{AC}(\omega)}{\varepsilon_0\omega} = \varepsilon_\infty + \frac{i}{\varepsilon_0\omega}\frac{\sigma_{2D}^{DC}}{1 - i\omega\tau}.$$

In accordance with BTS and BSTS, as well as the recent study,[5] we assume $\varepsilon_\infty = 1$.

S3 Dielectric function of hBN

Dielectric function of hBN is well-described by the TO-LO model where the in-plane and out-of-plane optical phonon modes described by a single Lorentzian oscillator model:

$$\varepsilon(\omega) = \varepsilon_\infty\left(\frac{\omega_{LO}^2 - \omega^2 - i\Gamma\omega}{\omega_{TO}^2 - \omega^2 - i\Gamma\omega}\right)$$

where ω_{LO}, ω_{TO}, Γ and ε_∞ are the LO and TO phonon frequencies, damping rate, and the high-frequency dielectric constant, respectively, having different values for the in-plane and out-of-plane directions relative to the atomic layers in a crystal.

The in-plane TO phonon frequency is measured by Raman spectroscopy shown in Fig. S1, providing the value of 1364.3 $\mathrm{cm^{-1}}$. This TO mode indicates to the isotopic composition of our hBN to be B^{10}:B^{11} = 20:80,[9] corresponding to the naturally abundant hBN crystal. This data is used to fit the TO and LO phonon frequencies for the out-of-plane dielectric function, providing the values reported in previous studies.[9-10] The remaining parameters (in-plane ω_{LO} and both ε_∞) are fitted using the dispersion of HPP in hBN on Si substrate measured by near-field imaging, as demonstrated in Fig. S2. These fitted values are also very close to reported in earlier works.[9] Phonon scattering energies Γ are adopted from previous studies.[9, 11-12] Parameters of the hBN dielectric function are summarized in Table S2.

		BTS	BSTS
Tauc-Lorentz	E_{01}, eV	1.69	1.94
	A_1	98	65.9
	C_1, eV	1.85	1.94
	E_{02}, eV	0.49	-
	A_2	41.1	-
	C_2, eV	0.16	-
	E_g, eV	0.24	0.25
	ε_∞	5	0
Drude	ω_p, eV	1.39	7.5
	Γ, eV	0.086	0.05
	ε_∞	1	1.3
	Layer thickness, nm	1.28	1.5

Table S1. Parameters of BTS and BSTS dielectric function used for modeling.

	ω_{LO}, cm^{-1}	ω_{TO}, cm^{-1}	Γ, cm^{-1}	ε_{∞}
In-plane	1619.8	1364.3	5.3	5.22
Out-of-plane	820.2	761.0	3	2.25

Table S2. Parameters of hBN dielectric function used for analytical modeling. Parameters fitted from the near-field dispersion measurements (Fig. S2) are shown in red.

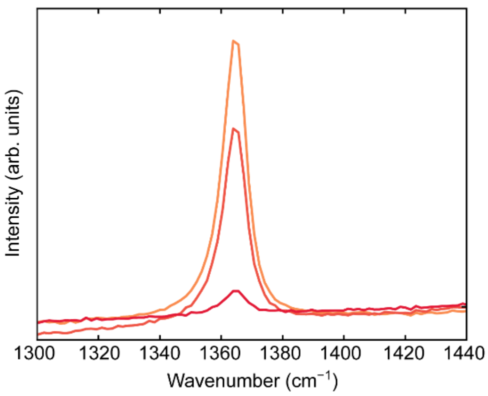

Figure S1. Raman spectra of three hBN flakes of different thickness, all providing the TO phonon frequency of 1364.3 cm^{-1}.

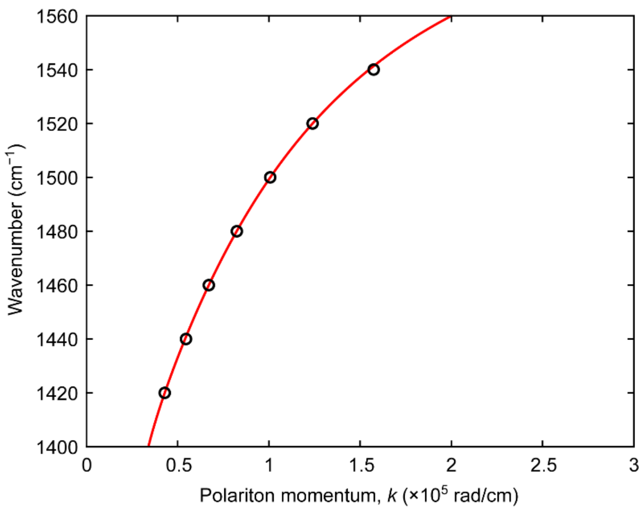

Figure S2. HPP dispersion in 105 nm-tick hBN on Si substrate: near-field experimental data (points) and fitted analytical dispersion calculated by using hBN dielectric function parameters provided in Table S2. The ~2 nm-thick native SiO_2 layer is confirmed to cause insignificant deviation of the HPP dispersion and is not accounted for during the fitting procedure.

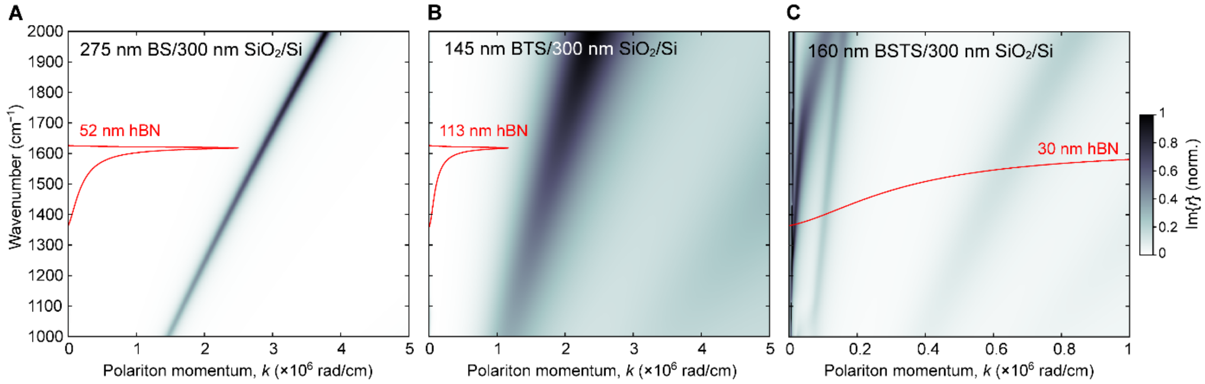

Figure S3. Analytically calculated dispersion of the plasmonic modes (color map) supported by the topological surface states in the continuous multilayer structure of TI materials on 300 nm SiO2/Si substrate (as noted). Conductivity of the surface layers is calculated using the Drude model with parameters listed in Table S1. Also shown: dispersion of the first-order HPP in hBN (red) on the corresponding TI material without conductive surface layers.

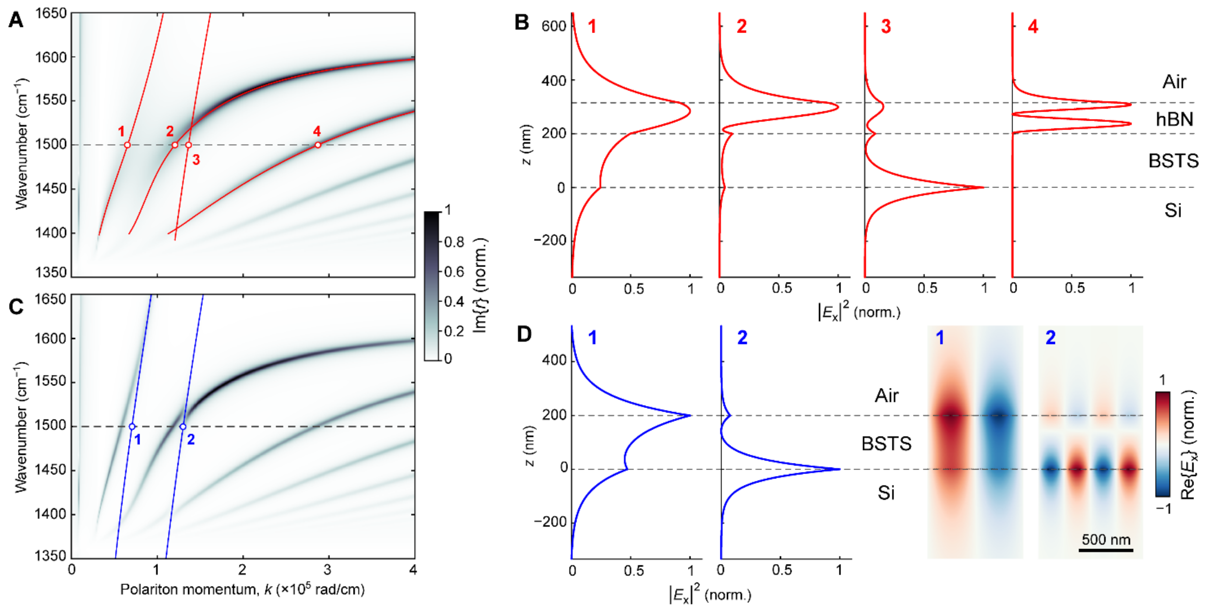

Figure S4. A Analytically calculated dispersion of the eigenmodes in the continuous multilayer structure of air / 115 nm hBN / 200 nm BSTS / Si, calculated for BSTS with the theoretically predicted surface states. Red curves show the exact dispersion solutions found in the structure, while the imaginary part of the reflection coefficient (color) maps the same modes. **B** Intensity profiles of the in-plane electric field calculated for eigenmodes shown in **A** at 1500 cm^{-1}, demonstrating hybridization of hBN HPP and plasmons supported by the BSTS surfaces (modes "1", "2", and "3") and the pure second-order HPP mode in hBN (mode "4") which does not hybridize due to momentum mismatch. **C** Color map: same as in **A**, but calculated with ten times lower ohmic loss in BSTS surfaces in order to clearly demonstrate the modes hybridization. Blue curves: plasmonic eigenmodes in the structure without hBN that hybridize with HPP as shown in **A** and **B**. **D** Field profiles of the plasmonic eigenmodes supported by 200-nm-BSTS on Si: the system with two 2D conductive surfaces supports two modes with opposite field symmetry. Note that the mode "1" fully hybridizes with HPP (also mode "1" in **B**), while the mode "2" weakly couples to HPP (modes "3" and "2" in **B**, respectively) due to the different field symmetry.

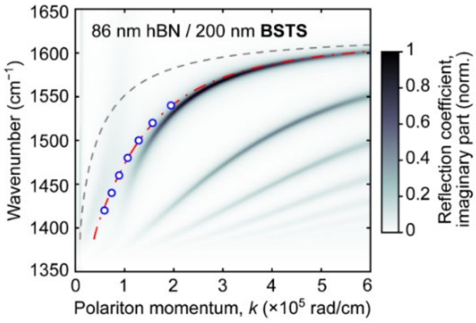

Figure S5. Dispersion of the eigenmodes in the continuous multilayer structure 86 nm hBN/BSTS/SiO_2: calculated considering BSTS with conductive surface layers (color map), without the surface layers (red dash-dotted), and experimentally measured (data points).

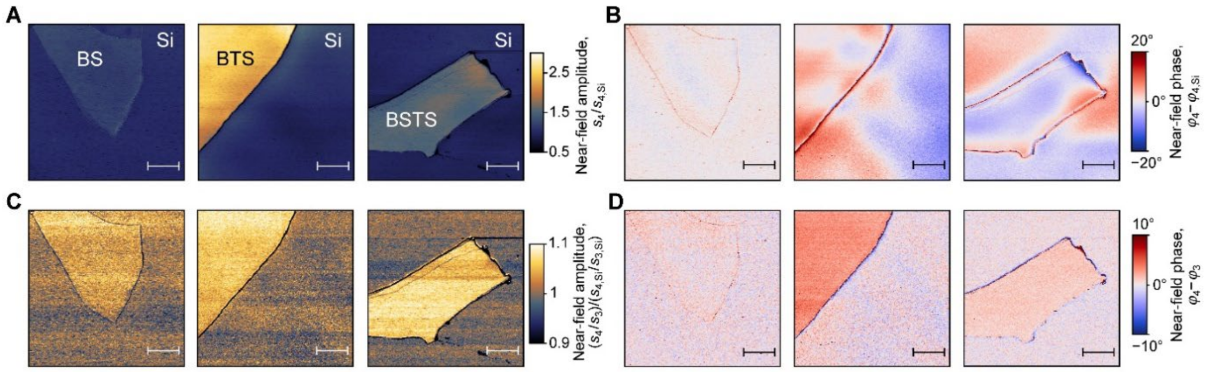

Figure S6. Same as Figure 5 in the main text for the excitation frequency of 1600 cm^{-1}. All scale bars are 2 μm.

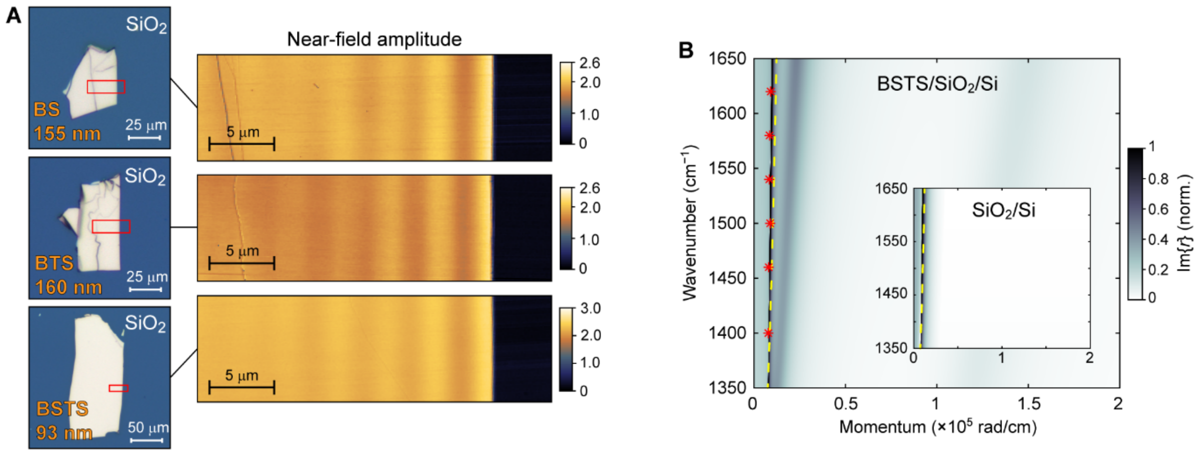

Figure S7. A Near-field images of the edge of TI flakes on SiO_2/Si substrate at the excitation frequency of 1500 cm^{-1}. **B** Imaginary part of the reflection coefficient (color map) of the BSTS/SiO_2/Si structure with topological surface states in BSTS, measured dispersion of the interference pattern visible in **A** over the BSTS flake (red symbols), and the light line in SiO_2 (yellow dashed). Inset: imaginary part of the reflection coefficient of SiO_2/Si, showing the same light line feature as in BSTS/SiO_2/Si. Measured dispersion considers the oblique incidence of the illumination beam to the sample surface which affects the period of the interference pattern, while the edges were orthogonal to the plane of incidence.

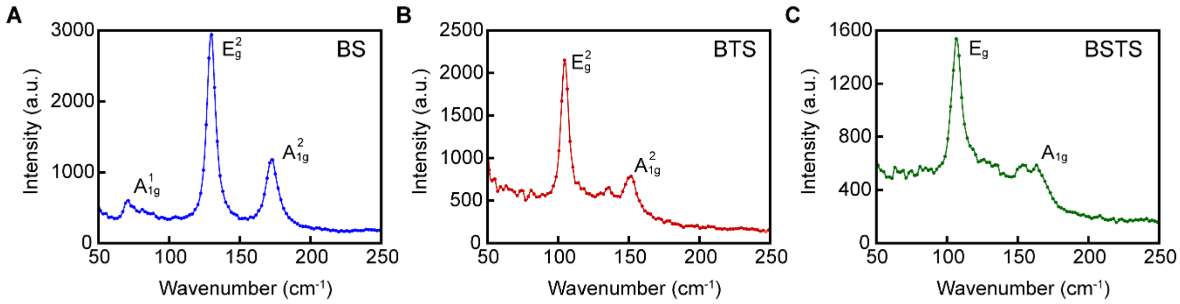

Figure S8. Raman spectra of the three TI materials used in experiments, excited at 514 nm. IR-active modes are indicated next to their peaks.

References

[1] P. K. Venuthurumilli, X. L. Wen, V. Iyer, Y. P. Chen, X. F. Xu, *ACS Photonics* **2019**, *6*, 2492.

[2] C. S. Tang, B. Xia, X. Q. Zou, S. Chen, H. W. Ou, L. Wang, A. Rusydi, J. X. Zhu, E. E. M. Chia, *Sci. Rep.* **2013**, *3*, 3513.

[3] J. Y. Ou, J. K. So, G. Adamo, A. Sulaev, L. Wang, N. I. Zheludev, *Nat. Commun.* **2014**, *5*, 5139.

[4] Z. J. Yue, B. Y. Cai, L. Wang, X. L. Wang, M. Gu, *Sci. Adv.* **2016**, *2*, e1501536.

[5] S. Chen, A. Bylinkin, Z. T. Y. Wang, M. Schnell, G. Chandan, P. N. Li, A. Y. Nikitin, S. Law, R. Hillenbrand, *Nat. Commun.* **2022**, *13*, 1374.

[6] K. W. Post, B. C. Chapler, L. He, X. F. Kou, K. L. Wang, D. N. Basov, *Phys. Rev. B* **2013**, *88*, 075121.

[7] M. Brahlek, N. Koirala, M. Salehi, N. Bansal, S. Oh, *Phys. Rev. Lett.* **2014**, *113*, 026801.

[8] J. Yin, H. N. S. Krishnamoorthy, G. Adamo, A. M. Dubrovkin, Y. D. Chong, N. I. Zheludev, C. Soci, *NPG Asia Mater.* **2017**, *9*, e425.

[9] A. J. Giles, S. Dai, I. Vurgaftman, T. Hoffman, S. Liu, L. Lindsay, C. T. Ellis, N. Assefa, I. Chatzakis, T. L. Reinecke, J. G. Tischler, M. M. Fogler, J. H. Edgar, D. N. Basov, J. D. Caldwell, *Nat. Mater.* **2018**, *17*, 134.

[10] J. D. Caldwell, A. V. Kretinin, Y. G. Chen, V. Giannini, M. M. Fogler, Y. Francescato, C. T. Ellis, J. G. Tischler, C. R. Woods, A. J. Giles, M. Hong, K. Watanabe, T. Taniguchi, S. A. Maier, K. S. Novoselov, *Nat. Commun.* **2014**, *5*, 5221.

[11] G. X. Ni, A. S. McLeod, Z. Y. Sun, J. R. Matson, C. F. B. W. Lo, D. A. Rhodes, F. L. Ruta, S. L. Moore, R. A. Vitalone, R. Cusco, L. Artús, L. Xiong, C. R. Dean, J. C. Hone, A. J. Millis, M. M. Fogler, J. H. Edgar, J. D. Caldwell, D. N. Basov, *Nano Lett.* **2021**, *21*, 5767.

[12] S. Dai, Z. Fei, Q. Ma, A. S. Rodin, M. Wagner, A. S. McLeod, M. K. Liu, W. Gannett, W. Regan, K. Watanabe, T. Taniguchi, M. Thiemens, G. Dominguez, A. H. C. Neto, A. Zettl, F. Keilmann, P. Jarillo-Herrero, M. M. Fogler, D. N. Basov, *Science* **2014**, *343*, 1125.